Journal of Building Engineering 77 (2023) 107521

Contents lists available at ScienceDirect

Journal of Building Engineering

journal homepage: www.elsevier.com/locate/jobe

Pneufin: A switchable foil cushion inspired soft pneumatic adaptive shading

Rakhmat Fitranto Aditra [a,b,*], Paolo Beccarelli [a], Robin Wilson [a]

[a] Department of Architecture & Built Environment, University of Nottingham, University Park, Nottingham, NG7 2RD, United Kingdom
[b] School of Architecture, Planning and Policy Development, Institut Teknologi Bandung, Jl. Ganesha 10, West Java, Indonesia

ARTICLE INFO

Keywords:
Soft pneumatic
Adaptive shading
Fabric membrane
Prototyping
Building simulation

ABSTRACT

Switchable foil cushion which has lower actuation pneumatic pressure compared to other soft pneumatic adaptive system. This lower pressure should be advantageous against leakage. The actuation principle of switchable foil cushion was compared to other soft pneumatic adaptive systems and applied into Pneufin: a soft pneumatic adaptive external shading. The actuation and structural performance were analysed through 2D and 3D simulation, and experiments using full-scale prototypes. The prototypes could be actuated with pneumatic pressure less than 1 kPa. While the simulation shows that the wing angular rigidity of Pneufin could be controlled by its pneumatic pressure, the experiment showed that its effectiveness is greatly affected by the dimension of the middle layer membrane. Building energy simulation showed that the shading effectiveness on building energy and daylighting performance were affected by the shading adaptability. The study findings expand the further study and design development for Pneufin.

1. Introduction

1.1. Research background

Active adaptive building system that could be actuated to adapt with the environment and building needs has been developed for a long time. It comes in various application, such operable windows to responsive BIPV. One of actuation system that could be used for active adaptive building system is soft pneumatic which utilizing flexible or expandable material actuated through pressurized air and/or vacuum suction [1,2].

Soft pneumatic adaptive system has two main advantages than mechanical adaptive system: (1) flexibility, and (2) lower maintenance. The use of flexible pneumatic system could be beneficial against external load. It was able to damp the external load through material deformation [3]. The less weight, less moving and rotating parts, and mechanical requirement of soft pneumatic system makes it less prone to failure and thus require less maintenance [1,4,5]. Compared to smart material such as shape memory material and piezoelectric materials, soft pneumatic system could provide larger actuation force and movement in addition to rigidity against external force [6]. But, Zarzycki [1] also mentioned the disadvantage of soft pneumatic system that it must be continuously pressurized due to unavoidable leakage. This leakage could be affected by the amount of pressure and complexity of the system.

There were a lot of projects and research about soft pneumatic adaptive system [1,4,7–9]. Soft pneumatic adaptive system has been reviewed in architecture as part of adaptive system [2,10–17]. Andric et al. [18] has reviewed soft pneumatic adaptive structure and experiments several modular configurations and its actuation characteristics. Hartz [4] categorized three type of movement from

* Corresponding author. Department of Architecture & Built Environment, University of Nottingham, University Park, Nottingham, NG7 2RD, United Kingdom.
E-mail addresses: rakhmat.aditra@gmail.com (R.F. Aditra), paolo.beccarelli@nottingham.ac.uk (P. Beccarelli), robin.wilson@nottingham.ac.uk (R. Wilson).

https://doi.org/10.1016/j.jobe.2023.107521
Received 17 May 2023; Received in revised form 21 July 2023; Accepted 5 August 2023
Available online 9 August 2023

air-inflated pneumatic structure.

The application soft pneumatic adaptive system ranged from sun shading, façade, to roof. Even in the same application as building façade, actuation pressure was also widely range from very low pressure (below 1 kPa) of switchable ETFE foil cushion [19] to high pressure (67.5 kPa) of Flexagon [7].

This low actuation pressure of switchable ETFE foil cushion became the impetus of this research and the development of Pneufin. In this paper, the difference in design principle between switchable ETFE foil cushion with the other soft pneumatics were explored. Then a Pneufin shading, as alternative soft pneumatic adaptive system inspired by switchable ETFE foil cushion design principle, will be suggested, analysed, and discussed in this article.

1.2. Research aims

This study aims to describe the design principle and kinematics of Pneufin. Pneufin is shaped like a vertical fin with pair of openable wings (Fig. 1). Pneufin was first introduced by Aditra et al. [20] as Switching Soft Pneumatic Adaptive System. This study aims to further analyse the potential of Pneufin in three aspects: actuation, structure, and building energy and daylighting performance.

As a moving building component, Pneufin actuation performance should be analysed. This stage is an important step in designing new soft pneumatic system as many soft pneumatic adaptive systems, even without any external load, has to resist its material deformation during its actuation [1]. By adopting the design principle of switchable ETFE foil cushion, Pneufin is assumed to have low actuation pressure.

As external shading, Pneufin would also be subjected to external load (wind). A soft pneumatic actuator usually has to find balance between increasing structural stiffness and lowering actuation force [21]. Thus, testing the structural performance is equally important as the actuation. In this research, the structural performance would be analysed based on equilibrium wind pressure. To approximate the dynamic behaviour of the wings, the structural test would be done on different wing angles.

The Pneufin has only 2 modes: Folded and Unfolded mode. The former is when the wing folded and allows the most solar radiation to enter the façade. The latter is when the wing unfolded and block the most solar radiation. It could not be actuated into intermediate angle. Thus, its individual fins would have a very limited adaptability compared to other SPAS [7,22] or other mechanical adaptive system [1]. A higher adaptability could be gained by controlling the fins separately. The hypothesis is that the more flexible the fins could be controlled, the higher the building energy saving would be. Thus, building energy simulation would be done to evaluate this hypothesis. Other than building energy, adaptability of the fins should also affect the daylighting. Controlling the fins to achieve lowest energy would affect illuminance of a building. Thus, in this paper, the effect of shading adaptability to the daylight performance is also analysed.

2. Method: development and analysis of Pneufin

2.1. Pneufin design principle

This study divided the soft pneumatic adaptive system into two types based on the actuation principle (Fig. 2). The first actuation principle is actuating a pneumatic chamber or collection of pneumatic chambers to transform the system to certain degree according to the volume or pressure of the pumped air [1,7,18,22–28]. During actuation, the SPAS system gets additional rigidity due to prestressed

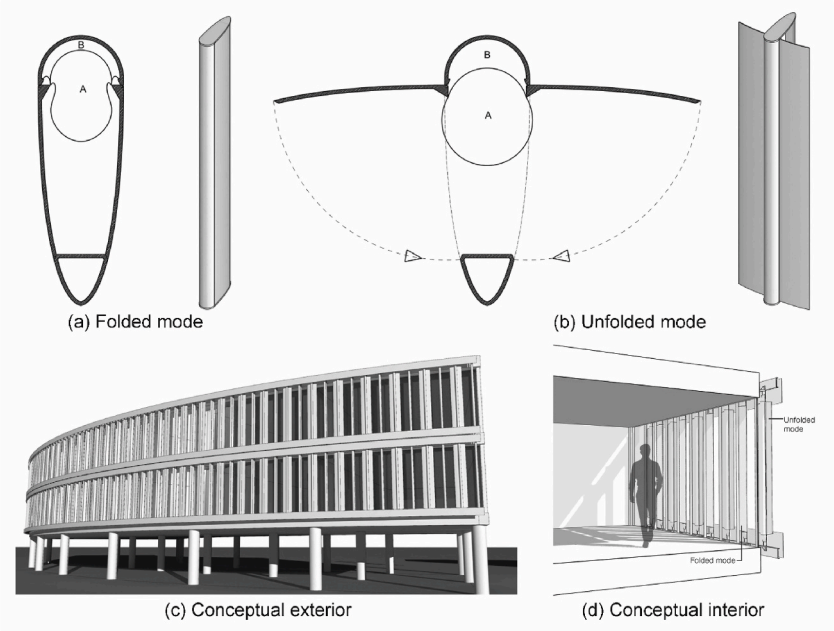

Fig. 1. Conceptual design of Pneufin.

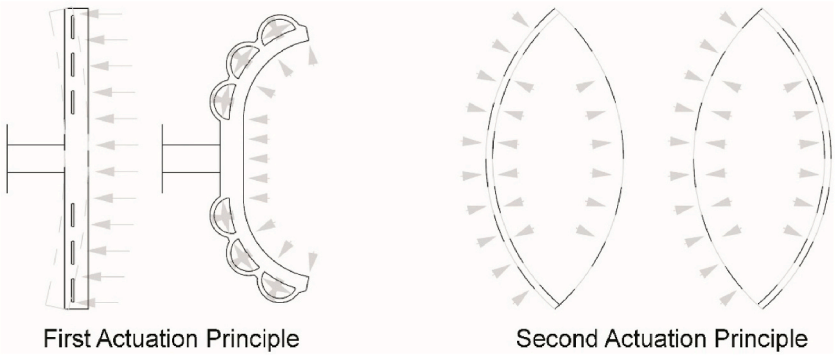

Fig. 2. Two different actuation principles.

system. But, during relaxed state, only the initial rigidity exists to withstand external load. This actuation principle was not only found in building system, but also in other application, such as soft robotics, or wing actuators [21,29].

In the first actuation principle, two methods are used to provide initial rigidity [20]: (1) semi-elastic material [1,7,22–25,27,28], or (2) counterweight [18]. These methods have two conflicting requirements: (1) High material rigidity or heavy counterweight for higher initial rigidity during relaxed state, and (2) low material rigidity for lower actuation pressure. The system with this principle needs to be actuated with increasing pressure until reaching its final shape.

Switchable ETFE foil cushion has the second actuation principles: the prestressed chamber is switched to actuate the cushion. Instead of having relaxed and prestressed modes, the switchable ETFE foil cushion is always air-prestressed in both modes. Thus, it does not need a semi-elastic material or counterweight that could hinder the actuation. With the ETFE foils relatively having no bending stiffness and not stretched during actuation, the actuation of switchable ETFE foil cushion is conceptually isobaric.

This second principle became the design principle for Pneufin, albeit with further interpretation: (1) having two prestressed modes, and (2) folded membrane instead of stretched during actuation. Pneufin consists of two chambers: Upper and lower chambers (A and B in Fig. 1, respectively). To open the shading (Unfolded mode), both chambers need to be pressurized at a same pressure, and to close the shading (Folded mode), the upper chamber needs to be vacuumed (negative pressure) while the lower chamber relaxes. This actuation would fold membrane around the wing hinges.

The three layers of the chambers have distinct roles. The upper layer is under tension during folded state and compressed during unfolded mode. Thus, it should be a rigid layer and, conceptually, would not give any force to the wings during actuation. The middle layer relaxes during Unfolded mode and under tension during Folded mode. Lastly, the lower layer behaves in reverse of the middle layer. All layers attach to a pair of wings which actuates accordingly. Each of the wings rotates on its hinge attached to the rigid upper layer and has lever to increase the actuation moment force.

2.2. Prototype for experiment

Two prototypes were made to evaluate the actuation and structure performance. While those were one-to-one scale prototype, the purpose of it was for experimental purpose rather than real world application. The prototypes were an updated version of prototype used in Ref. [20] (Fig. 3).

Both prototypes consisted of two parts: pneumatic tube and rigid part. The pneumatic tubes were 3-layer polyurethane coated nylon membrane with a half steel pipe in the between of upper and middle layer. The difference of Prototype 1 and 2 was only on the dimension of the middle layer membrane. The Prototype 1 middle layer membrane section arc has circumference of 86.71 mm. Meanwhile the Prototype 2 was 115.65 mm (Fig. 4).

The rigid part was 3D printed and redesigned several times. The rigid part consisted of chamber shell, chamber frame, and wing frame. The chamber shell and frame are attached to the aluminium extrusion and clamp the pneumatic tube. Together with the half steel tube inside the pneumatic tube, it acts as the rigid upper layer of the pneumatic chamber.

Both the chamber frame and chamber shell were mainly made from 3D printed PLA. Chamber shell functioned as the main support of Pneufin. It gripped both the pneumatic tube and the aluminium extrusion. The chamber frames did not directly connect to aluminium extrusion. Instead, it was secured in its position by a sets of 2 mm carbon rods that passed through the chamber frame and chamber shell. Includes in the chamber frame is the wing hinges where the wing frames attached. Attached using carbon rod. The wing hinges were made from water-jet-cut steel plate that were joint with the 3D printed PLA parts with brass dowel (Fig. 3).

The wing frame functions as lever which translates the smaller movement and higher force of the pneumatic tube into bigger movement and lower force of the wing. The wing frame consists of (1) horizontal frame, (2) clamp and lever, and (3) threaded steel rod. The model of the prototypes is supplied in the Additional Files.

2.3. Actuation

Conceptually, Pneufin could only be actuated to fully unfolded or folded mode. But, from the early actuation test [20], folding resistance still slightly plays role on the wing actuation, thus different chamber pressure could change the wing position.

Actuation procedure of Prototype 1 and Prototype 2 was same. The aim of the actuation test was to find the lowest pressure or

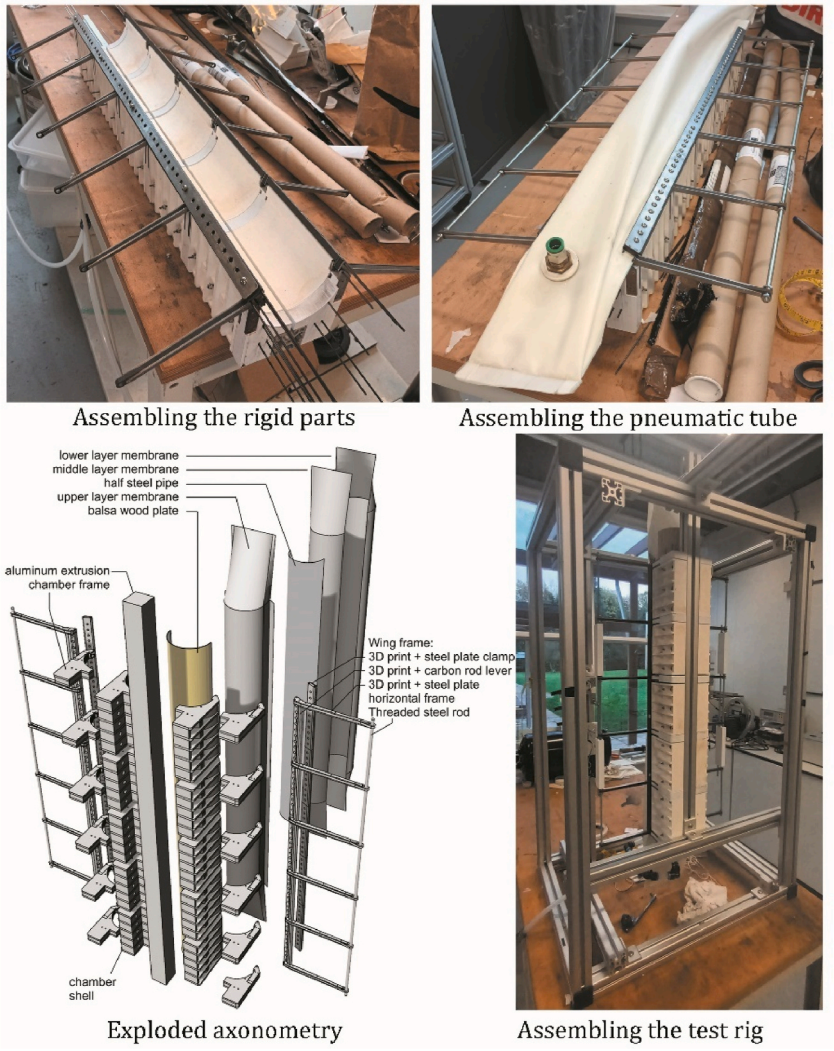

Fig. 3. Prototype construction.

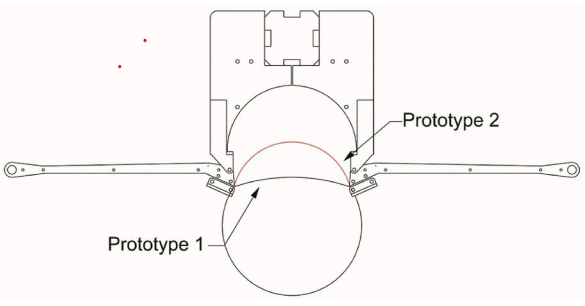

Fig. 4. Section of the prototypes.

vacuum to actuate the prototypes. Fig. 5 shows the actuation experiment setup. A flow control valve and a valve were used to control the pressure in the system while the pump was activated.

First, the wings were positioned on relaxed position, then the arbitrary pressure/vacuum was tested. After that, whether the wing tip reached the intended position or not was recorded. According to the wing position result, the step was repeated with different pressure. If the wing reached the intended position, the pressure or vacuum was decreased. If the wing did not reach the intended position, the pressure or vacuum was increased. The procedure was repeated until no lower pressure or vacuum that could made the wing reached the

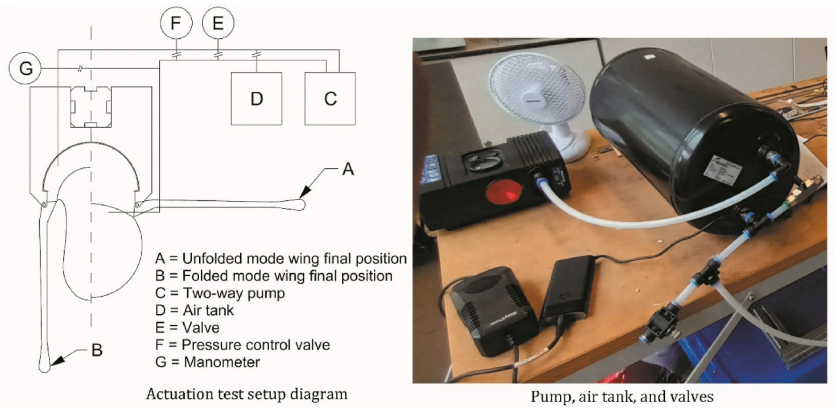

Fig. 5. Actuation experimental setup.

intended position could be achieved. A of actuation experiment procedure of each mode is supplied in the Additional Files.

2.4. Structural performance

Structural analysis purpose is to see how the Pneufin would withstand external load, such as wind load. This paper represents the wind load by equilibrium wind pressure ρ_w. Equilibrium wind pressure ρ_w defines the max wind pressure the pneumatic pressure could withstand moment equilibrium with. Equilibrium wind pressure was assessed through three methods: Analytical method, Experiment, and Finite Element Analysis.

The direction of wind pressure is flipped for each mode: inward for Unfolded mode and outward for Folded mode. The reversed direction of wind pressure was not assessed because the assumption that it would be resisted by wing hinge, instead of the pneumatic tube.

2.4.1. 2D analytical method

2D Analytical method was based on rigid body moment equilibrium equation (Eq. (1) and Fig. 6) scripted in Grasshopper® of Rhino3D [30]. The equation assumed that, in equilibrium state, the wind load moment (M_w) would be same with combination of moment of lever force (M_l) and hoop stress (M_h).

$$M_w = M_l + M_h \quad \text{Eq. 1}$$

Moment force on the lever M_l was calculated from pressure force in lever area f_l (Eq. (2)). Moment force due to the hoop stress moment M_h was calculated with Eq. (3). Hoop stress σ_h is a function of pressure ρ_m, radius r, and thickness t of the membrane. The assumption of this hoop stress equation is that no significant longitudinal internal membrane force that pulls the tip of the lever.

$$M_l = f_l \bullet 0.5 l_l = \rho_m \bullet h_l \bullet 0.5 l_l^2 \quad \text{Eq. 2}$$

$$M_h = f_h \bullet l_h = \sigma_h \bullet t \bullet h_l \bullet l_h = \rho_m \bullet r \bullet h_l \bullet l_h \quad \text{Eq. 3}$$

To find the wind pressure ρ_w from wind load moment, the wing section was first divided into twenty segments. Then Eq. (4) was used which defines the moment on wings as incremental moment M_{wi} on each wing segment. It calculates the wing moment arm l_{wi}, wing height h_w, and wing segment length Δl_w from the wing design.

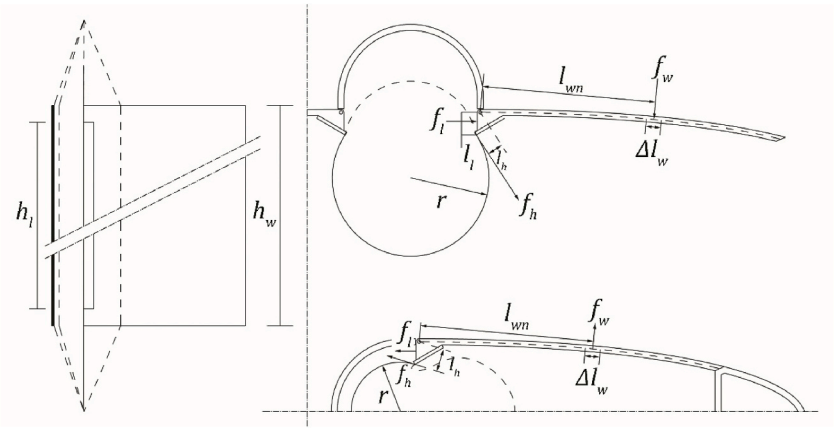

Fig. 6. Vertical section (Left), Unfolded mode (Upper right) and Folded mode (lower right) plan.

$$M_w = \sum_{i=1}^{20} M_{wi} = f_{w1} \bullet l_{w1} + f_{w2} \bullet l_{w2} + \ldots + f_{w20} \bullet l_{w20} = \left(\sum_{i=1}^{20} l_{wi} \bullet \Delta l_{wi} \right) \bullet \rho_w \bullet h_w$$

$$\rho_w = M_w \Big/ \left(\left(\sum_{i=1}^{20} l_{wi} \bullet \Delta l_{wi} \right) \bullet h_w \right) \quad \text{Eq. 4}$$

To simulate at different wing angle, an additional script based on Eqs. (5) and (6) updates the section of membrane accordingly. The rotation of the wings $\Delta\theta_w$ would change the section half-opening t and the height h of the chamber section (both modes) (Fig. 7).

Equations (5) and (6) explain the relation between the fully unfolded/folded section opening angle θ_1 , targeted section opening t_2, and resulting section opening angle θ_2 and height h_2. Equation (5) is a numerical problem. Rather than manually testing different geometry, interpolation method was used.

The interpolation was done by testing ranges of the θ_2 with right-hand side of Eq. (5). A spline interpolation curves were made from the result of both modes. The questioned θ_2 for each mode was found by testing the left-hand side of Eq. (5) in the interpolation curve. Then the h_2 could be found by solving Eq. (6). At last, new section was created from the new height h_2. The script is provided in the Additional files.

$$\frac{\theta_1 \times r_1}{t_2} = \frac{\theta_2}{\sin\theta_2} \quad \text{Eq. 5}$$

$$h_2 = \frac{t_2}{\sin\theta_2} + \frac{t_2}{\tan(\pi - \theta_2)} \quad \text{Eq. 6}$$

2.4.2. Experiment

Fig. 8 shows the setup for the structural experiment. The eleven chamber pressures were tested for each prototype. To get the wing

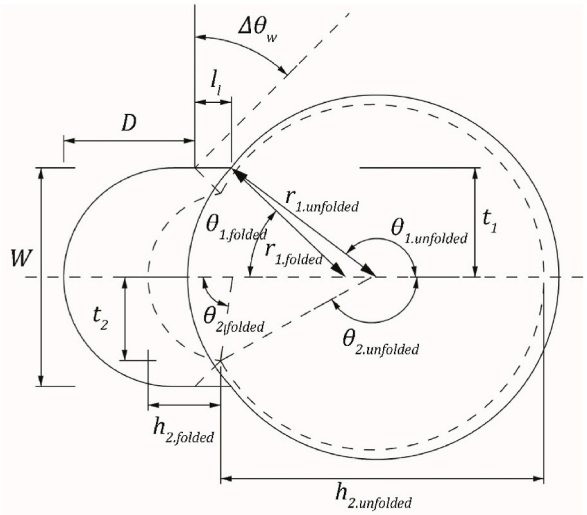

Fig. 7. Wing angle to chamber section.

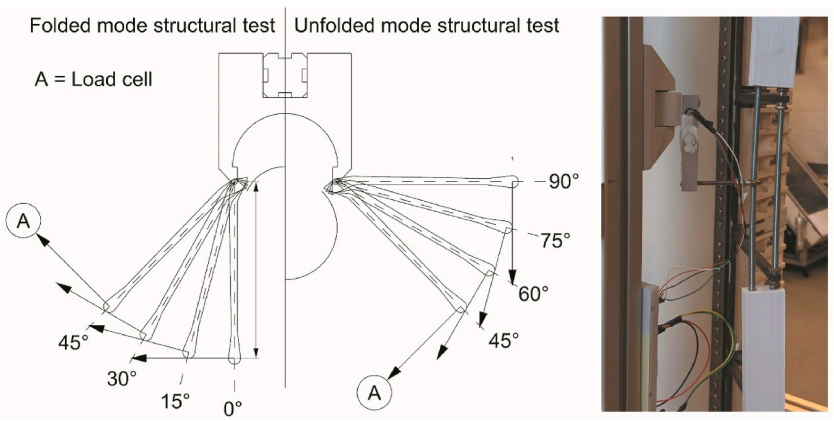

Fig. 8. Structural Experiment setup.

reaction load, an Arduino load cell was attached to each wing. Each mode was assessed with four wing angle position. The wing reaction load results were then used in Eq. (4) and Eq. (7) to find the equivalent wind pressure.

$$M_w = l_w \bullet F_r \quad \text{Eq. 7}$$

The Arduino load cell was attached to the 3D printed rotatable holder to allow for different wing angle despite the orthogonal aluminium frame. To calibrate it, the load cells, also attached to the holder, were positioned horizontally. Then, weights were used as the calibration samples (Fig. 9 left). The weights weight was already tested in a laboratory scale.

The pressure ranged from 0 to around 11 kPa with around 1 kPa increments (negative and positive, for Folded and Unfolded mode, respectively). In some cases of Folded mode test, vacuum more than −10 kPA could not be achieved, especially if the pump has been activated for extended period. The pneumatic pressure was measured using manometer. In each pressure samples, the pump was remained activated. Once the pressure stabilized (wiggled around 0.01 kPa for the compression and 0.03 kPa for the vacuum), the pressure and wing reaction load was recorded manually (Fig. 9 right). A sample of the pressure and reaction load recording are supplied in the additional files.

2.4.3. Finite Element Analysis

The 2D analytical method had not considered the 3-dimensional effect of cap of the pneumatic chamber, and membrane deformation. Finite element analysis was used to simulate these parameters and to compare with the experiment results. Finite element analysis was done in FEM software RFEM DLUBAL [31].

The model material was based on experiment setup (Fig. 10). The membrane was modelled as typical coated fabric with warp and

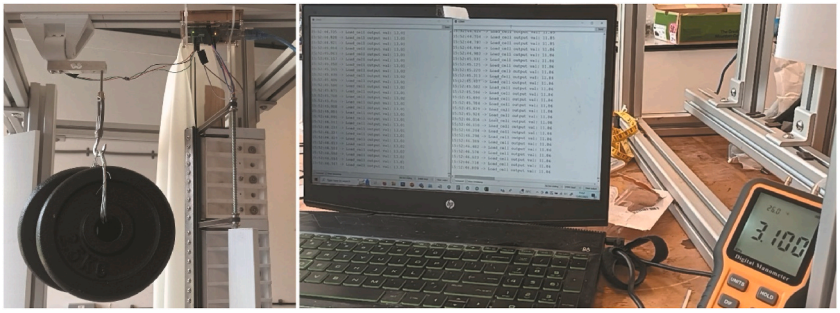

Fig. 9. Load cell calibration (left), and preview of structural experiment (right).

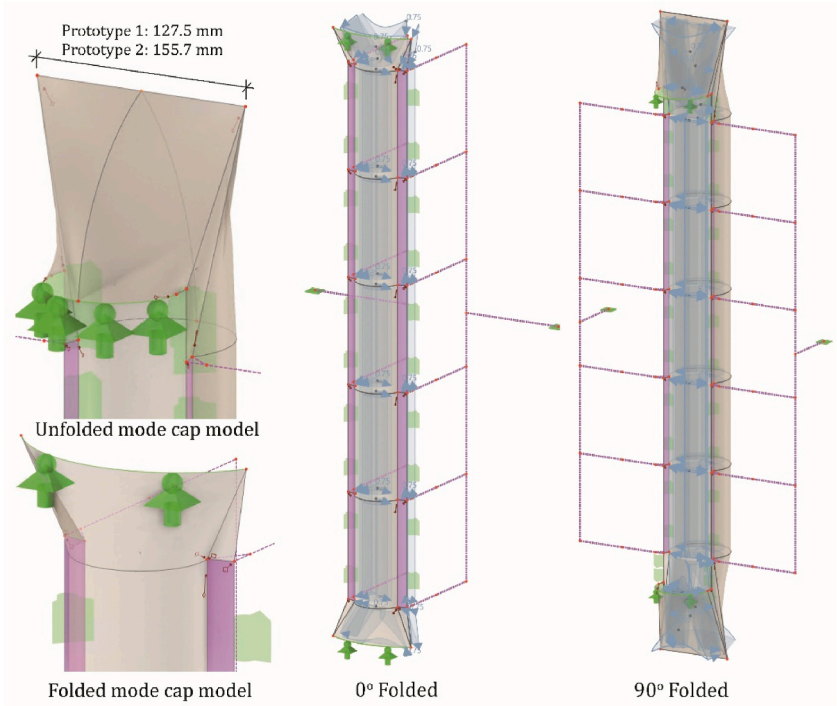

Fig. 10. FEM model input.

weft modulus elasticity of 1220 and 810 N/mm^2 and possio's ratio of 0.753. The wing model was simplification of wing frame. The wing was modelled as rigid wing assuming no significant deformation during the test. For both prototype model, the horizontal member was rigid to simplify the model. The same setup (wing angle, load cell position, and pressure ranges) from the experiment were assessed for each mode. The resulting reaction load were also converted to wind pressure with Eq. (4) and Eq. (7).

The difference of Prototype 1 and 2 FEM model was based on the experiment, which was mainly the middle layer membrane. The middle layer membrane should only under tension in the Folded mode. Thus, the different middle layer membrane was only modelled in Folded mode test.

The width of the cap welded part was also affected by the middle layer membrane. The cap was made by squeezing and welding the edge of each layer. Since the middle layer membrane of the Prototype 2 was wider, the cap welded part was also wider (Fig. 10).

In the FEM Unfolded model, the width of the cap was designed according to the prototype. On the other hand, the FEM model for the Folded mode have simpler cap. Based on the experiment, the cap was squeezed during Folded mode. It means that only a portion of the cap was under tension during this mode. Thus, the cap of the Folded mode was simply an outward extension of the middle layer membrane (Fig. 10).

2.5. Building performance simulation

2.5.1. Case study

The case study is a room on the second floor of a 3-story shophouse in Jakarta, Indonesia (Fig. 11). The room has 5-m front width, 4-m depth, and 3-m total height. Though it is a shop house, both storeys as used as office, as how it is usually happened in Indonesia. The building faces west and its façade is enclosed with the ten fins of Pneufin. The room is surrounded between neighbouring rooms and shophouses on all side, except the front side.

Four models with different shading adaptability, with addition of two static case (Folded and Unfolded mode) were compared. Adaptability was modelled as number of groups. A group is a collection of fins that is actuated together. The higher the number of groups is, the higher the adaptability. For example, if the shading is only composed of single group, then it has only 2 (2^1) options: all the fins folded or unfolded. If the shading is divided into two groups consist of five fins, then it has 4 (2^2) options: (1) all the fins folded, (2) first group folded while second group unfolded, (3) first group unfolded while second group folded, and (4) all fins unfolded. The number of mode options and groups arrangement is summarised in Table 1.

2.5.2. Building energy simulation

To simulate the lighting and cooling energy, a building simulation was done in Honeybee [32] then Energyplus to set some specific setting that could not be accessed through Honeybee. The simulated room is the front 5 × 3 m^2 room which programmed as an office. All of material used the based on standard material in Honeybee and Energyplus such as Ashrae 90.1 2010. Some of material with available data were adjusted based on Indonesian market or standard. The wall and window were modelled with material according to Indonesian standard [33] and research using specific Indonesian material [34,35]. The wall was a brick construction which has lower thermal resistance than the typical exterior wall in Energyplus, and the window was also based on single glazing clear glass window.

To simplify the simulation, the internal walls, ceiling, and floor were modelled as adiabatic surfaces, assuming the same conditioned temperature on the ground floor and the neighbouring shophouses. The shading was modelled as external shading of Energyplus. Table 2 summarizes the simulation parameters. Other parameters that are not mentioned in the table was based on the default setting of Energyplus. Some are updated with Ashrae 2017 Handbook of Fundamentals which Indonesian standard often refers itself to it. If the data is available, also updated with Indonesia standard, such as lighting electricity and heat gain, people heat gain, and minimum ventilation.

To simulate the adaptive façade, method similar to Ref. [8] was used. All mode options were simulated in Honeybee and Energyplus

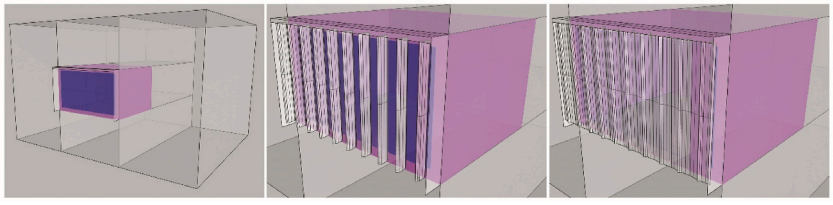

Fig. 11. Building energy simulation case study (left), Folded fins (middle), and Unfolded fins (right).

Table 1
Adaptability model and group arrangement.

Models	1 group	2 groups	3 groups	5 groups
Mode options	2 modes	4 modes	8 modes	32 modes
Groups arrangement[a]		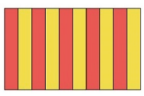		

[a] Front elevation. The fins with the same colour are one group.

Table 2
Building energy simulation parameters.

Office envelope	
External wall	Based on Ashrae 90.1 2010 typical insulated exterior mass wall, with adjustment based on [33,34] based on: - $R_e = 0.213$ - Thermal absorptance = 0.9 - Visual and solar absorptance = 0.3
Interior wall	Adiabatic – Same external wall material
Ceiling	Adiabatic – Generic Energyplus construction
Floor	
Window	based on [35]: U value = 4.94 Shgc = 0.82 T visual = 0.89
Lighting	LED [36,37] 8 W/m2 [38] Fractions [39]: Vis: 0.2, Conv.heat: 0.8, Rad: 0.0 350lx threshold [40]
HVAC (cooling)	Setpoint: 26.7 Celsius [41] Cooling to Electric E. (EER) = 3.5 [42]
People	Occupancy: 12 m^2/person [43] People gain: 132 W per person, (0.11 radiant, 0.55 sensible fraction) [41]
Equipment	14.35 w/m2 (0.25 radiant fraction) [43]
Infiltration	1.86×10^{-4} m3/s.m2 at 4 PA [43]
Ventilation	0.005 m3/s per person [41]

and then the results were collected. After that, the result was processed using Microsoft Excell and Grasshopper script to select mode of each hour with the lowest cooling and lighting electric energy.

The extracted result for this study is illuminance, cooling, and lighting electric energy. To get the cooling electric energy, the cooling energy result were converted into cooling electric energy with the EER of 3.5, which are the average of Indonesia AC market [42]. For lighting, the room was assumed to utilise 8 W/m^2 dimmable LED lamp which is the most used lamp type in Indonesia [36,37]. The lighting was also assumed to be adaptively and continuously dimmed according to the level of illuminance in the room.

Daylight performance indicator used in this paper is the time-fraction daylight autonomy (DA), which is the fraction of occupied times in a year during which minimum, task specific illuminance threshold achieved by daylight alone. In this simulation, illuminance threshold used is the same as the threshold used in the daylighting control: 350 lux (DA_{350lx}) and the total annual working hours of

Fig. 12. Folded mode (right) and Unfolded (left) mode actuation test.

2600 h. The threshold of 350 lux was based on SNI 03-6197-2000 (Indonesian standard about lighting energy efficiency) [40]. Illuminance value was acquired through 20-points illuminance map. The illuminance value of model was then analysed in Microsoft Excel. The DA_{350lx} of each point of each model were then compared to each other.

3. Result

3.1. Actuation

Fig. 12 shows the Folded and Unfolded mode actuation test. The wings kept its final positions as the pressure increased. Table 3 summarised the lowest pneumatic pressure/vacuum which the wing reaches its final positions. It shows that Prototype 1 has higher actuation pressure needed than Prototype 2.

3.2. Structural performance

3.2.1. Prototype 1

The Prototype 1 Folded mode structural test results (Fig. 13) shows linear correlation between Pneumatic and wing pressure. It also shows that the gradient increases as the wing open back during Folded mode.

In all angles, FE analysis result is higher than the other methods. Compared to the analytical results, the gradient from FE analysis always higher (21.5–23%) at all angles. It shows that the model of cap used in the FEM for the Folded mode increased the angular rigidity.

Meanwhile, the experiment result gradients compared to other methods changes in different wing angles. At 0° angle, the experiment result shows the lowest gradient. Other than that, it also has lower intercept than the rest. Which means if the line is

Table 3
Actuation pressure result.

	Prototype 1		Prototype 2	
	Folded mode	Unfolded mode	Folded mode	Unfolded mode
Lowest pressure/vacuum to actuate	−0.63 kPa	0.617 kPa	−0.41 kPa	0.48 kPa

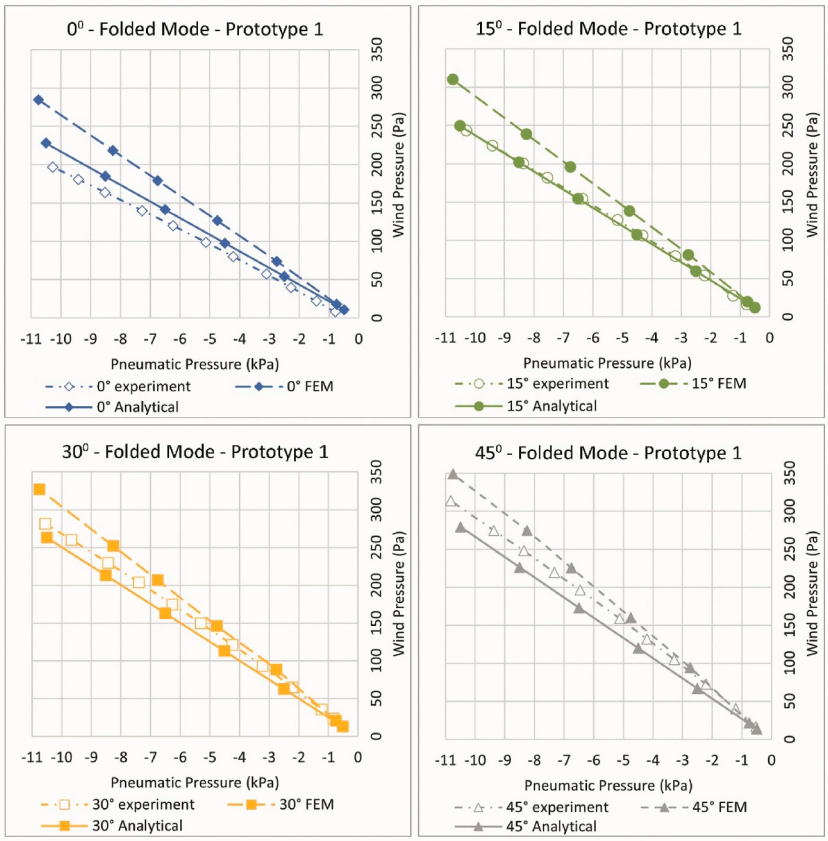

Fig. 13. Folded-Prototype 1 structural analysis result; Analytical, FEM, and experiment method.

extrapolated to zero wing pressure, the pneumatic pressure required is smaller negative pressure than the rest of method. At 15° angle, the experiment shows similar result with the analytical. At 30° and 45° angle, the experiment result gradients are higher than the analytical but still lower than the FEA result.

The Prototype 1 Unfolded mode structural test (Fig. 14) shows that the wind pressure Prototype 1 can withstand during Unfolded mode increases as the pneumatic pressure increases. It also shows that this correlation increases as the wing folded back during Unfolded mode. Analytical method results are the lowest among other method in all tested angles. The FE method results are slightly higher than the analytical method.

The experiment results show significant difference between each wing angle assessed. On the 45°–75° wing angle, the results were far higher than the rest of the method. The gradient difference also increased as the wing folded back (39%–79% higher than the analytical). On the other hand, the 0° wing angle result curved. It starts higher than the other method. Then, it curved until it got lower than the analytical method at around 7.5 kPa.

3.2.2. *Prototype 2*

The most striking difference Folded mode structural experiment result of the Prototype 2 compared to the Prototype 1 is the stagnating wind pressure on higher vacuum (<−5 kPA) (Fig. 15). The vacuum which the wind pressure started to stagnate increased as the wing angle increased (−6 kPA to −8 kPA).

The experiment result on lower vacuum range showed same pattern with the Prototype 1 in its comparison with the simulation. It started lower than the FEM result and increased as the wing angle increased. The FEM and analytical method showed that wind to pneumatic vacuum ratio of the Prototype 1 Folded mode was intended to be decreasing as the wing angle increases (0.0287–0.0244 for the FEM and 0.0241 to 0.0207 for the analytical method). But the experiment result showed increasing trend, especially during the lower vacuum (0 to −5 kPa) similar with the Prototype 1 Folded mode structural test (0.0237–0.0252).

The FEM and Analytical method result of the Prototype 2 Unfolded structural test was similar with the Prototype 1 (Fig. 16). The experiment on wing angle of 45°–75° was also similar with the Prototype 1. This suggested that the cap width do not affect the wind to pneumatic pressure ratio significantly.

The more significant difference between the prototype could be seen in the fully (90°) Unfolded mode. The curved pattern of the 90° Unfolded structural experiment was not appeared in the Prototype 2. Same with the rest of the different wing angle test, it kept its linear pattern from 0 to ±10 kPa pneumatic pressure.

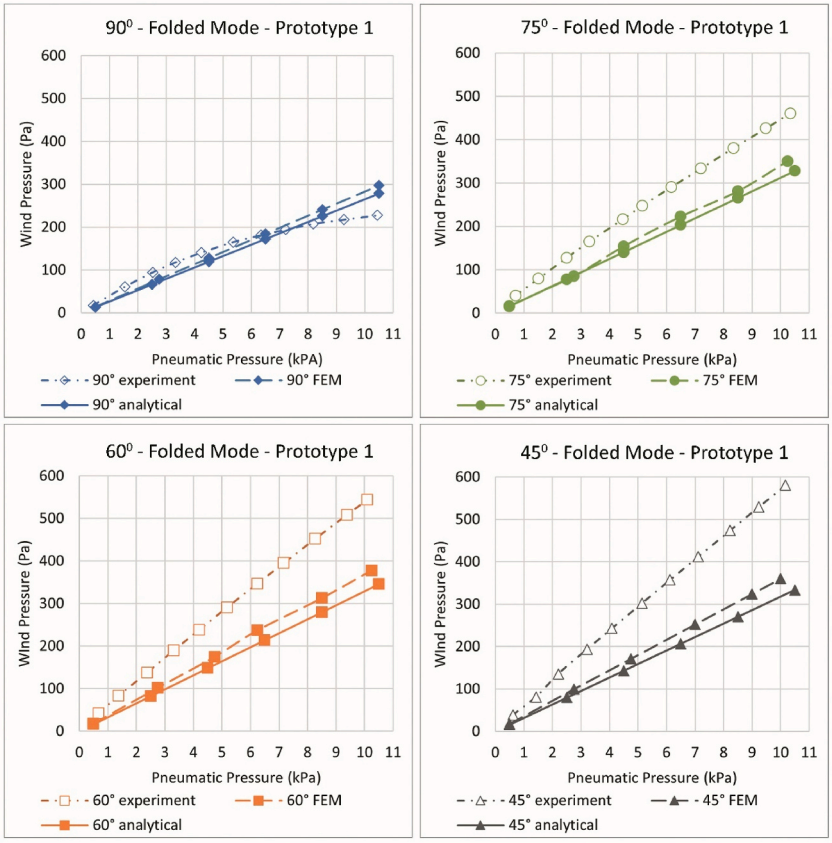

Fig. 14. Unfolded-Prototype 1 structural analysis result; Analytical, FEM, and experiment method.

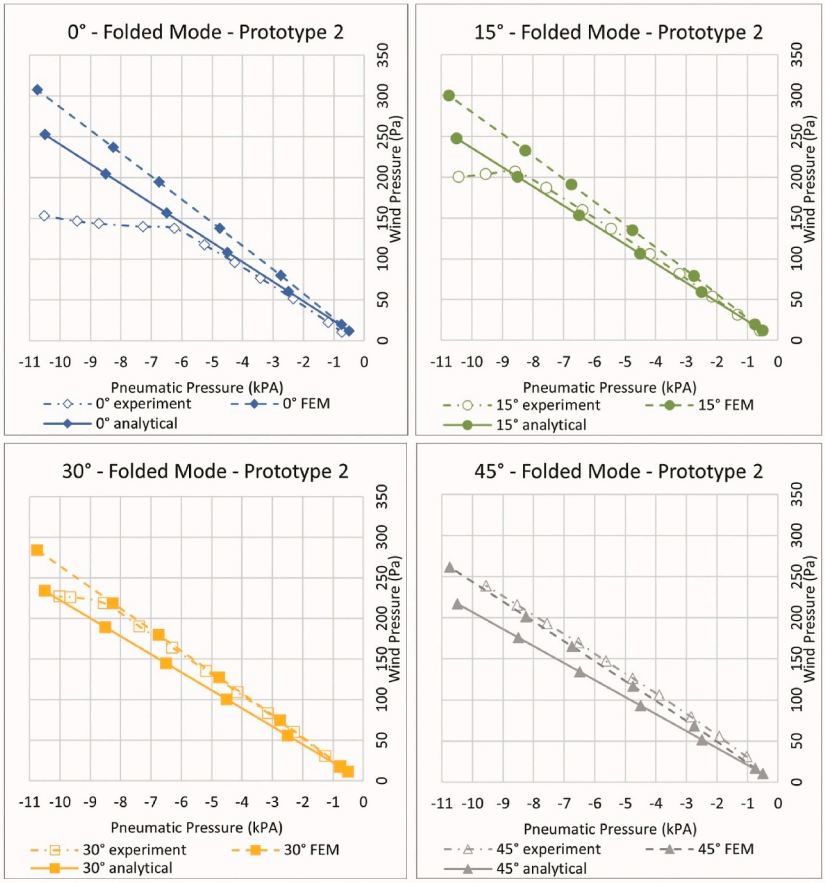

Fig. 15. Folded-Prototype 2 structural analysis result: Analytical, FEM, and experiment method.

3.3. Building energy simulation

In total (lighting + cooling), the adaptive models had lower electricity needed than the static ones. The lighting electricity was highest in Unfolded mode and lowest in Folded mode. The adaptive models' lighting electricity ranges in between. The pattern was also correlated with daylight autonomy (Fig. 17).

The same pattern is not found in the cooling electric energy. The cooling electric energy of adaptive models is even lower than the Unfolded, albeit not significant. This is despite the higher transmitted solar radiation (assumed from the lighting electricity) of the adaptive models. The increases in the lighting heat gain of the unfolded mode should also not exceed the decrease of window heat gain. Since the simulated HVAC did not have heat recovery, it suggests that the outdoor air heat gain of the Unfolded mode case was higher than the adaptive cases.

The total electricity from cooling and lighting decreases as the adaptability increases. The least and the most adaptable among the adaptive models decrease the electricity from cooling and lighting up to 11,03% and 29.44%, respectively, compared to the static Folded mode model.

Among the adaptive models, the cooling electric energy does not differ significantly. The 1 group model has 29.54% less cooling electricity compared to the Folded model. The 5 groups model has 32.28% less cooling electricity.

On the other hand, the lighting electricity of the adaptive models are significantly different among each other. The 1 group model has 4.58 times higher lighting electricity than the Folded mode. Meanwhile, the 5 groups model lighting electricity is only 1.27 times higher than the Folded mode.

Fig. 18 (left) shows similar average DA_{350lx} pattern with the lighting electric energy. Folded and Unfolded mode has extreme DA_{350lx} value of 100% and 0%, respectively, meanwhile the DA_{350lx} of adaptive mode increased as the adaptability increases. While the other adaptive mode shows almost distributed DA_{350lx} value of each map points, the 5 groups mode shows DA_{350lx} value ranges from 85% to 96%.

4. Discussion

4.1. Actuation

The difference of the Prototype 1 and 2 was only on the middle layer membrane. Thus, it was hypothesized that the actuation

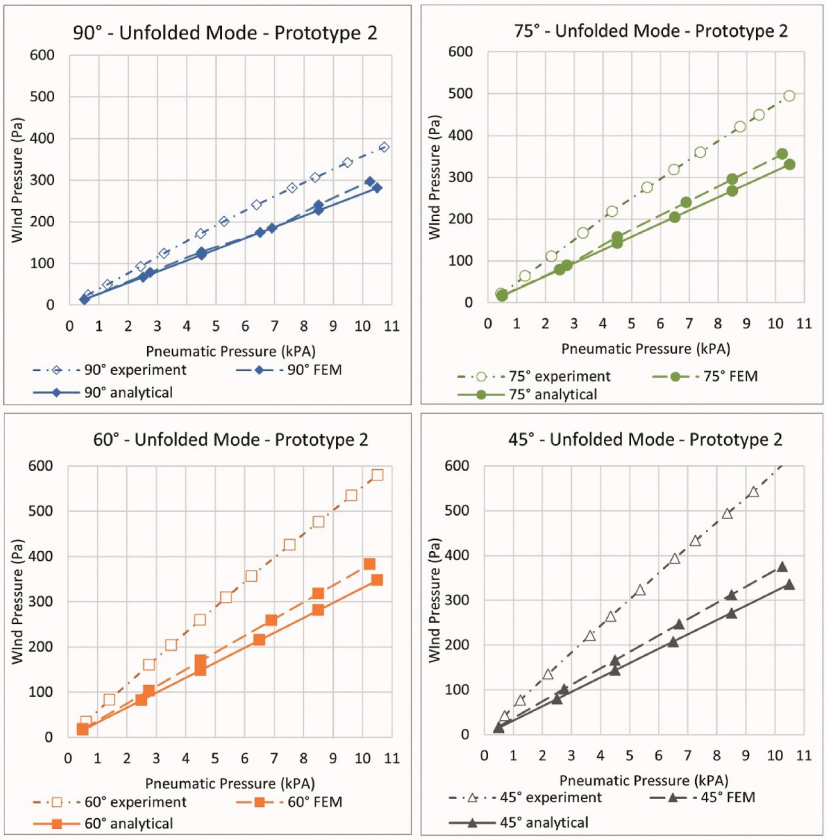

Fig. 16. Unfolded-Prototype 2 structural analysis result: Analytical, FEM, and experiment method.

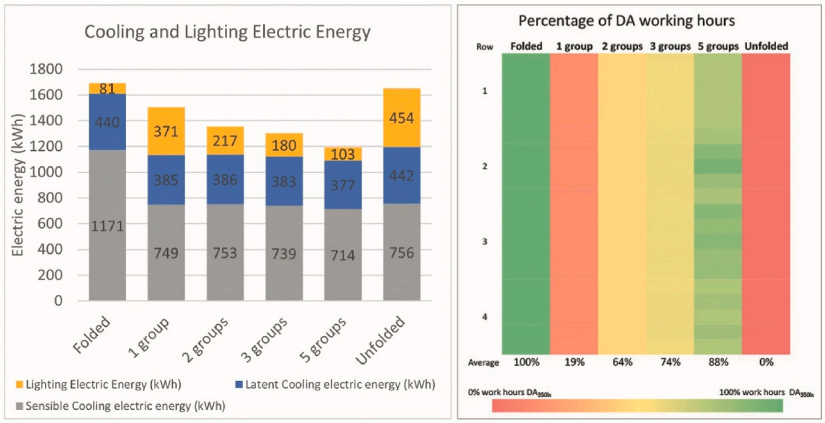

Fig. 17. Building energy (left) and Daylight performance (right) result.

pressure should only be different between the Folded modes only. But the result shows that the Prototype 2 have lower actuation pressure and vacuum than the Prototype 1.

This might be due to the different construction execution of each prototype. Even though the rigid components were the same on both prototypes. The carbon rods for the hinges were renewed in the Prototype 2. Other than that, controlling pressure below $\pm$ 1 kPA was difficult. Since both prototypes could be actuated below 1 kPA, concluding any difference between them would not be necessary.

The actuation result shows that, by applying the principle used in switchable fritted foil cushion [24], SPAS with low pressure actuation (without external load) could be designed. Another SPAS that used the same principle, such as the Breathing skin [44], also used very low actuation pressure.

But other actuation characteristic of Pneufin also showed implication of adopting the switching principle. In the actuation

experiment, the actuation from one mode started from its relaxed position, instead of from the other mode. This caused sudden movement during the actuation especially from the Folded mode to Unfolded mode. When the prototype relaxed from the Folded mode, the wing suddenly moved to its half-folded position due to the folding resistance of the lower membrane.

This did not visualize how the actuation in real-world application quite well. In real-world application, each the inflation system should directly switch to different mode, without relaxing the pneumatic tube first. To approximate the real-world actuation, an aesthetic prototype was made. It used the Prototype 1 pneumatic tube, and switched the wings that approximate the geometry of real-world Pneufin application. Unlike the experiment prototype, the actuation of this prototype was started from the prototype still retaining the previous mode pressure/vacuum. The movement of the wings suggested that the smoothness of Pneufin actuation relies solely on the construction. It is the most visible during the Unfolding actuation which one of the wings move faster than another wing (Fig. 18). The recording of this actuation is also provided in the additional files.

Furthermore, it was also apparent that during the transition to each mode, the wings had no angular stiffness from the pneumatic tube. Actuation of one shading could be done in just under 30 s, but if multiple Pneufin are actuated simultaneously, then those would have no angular stiffness for an extended period. Therefore, automatic actuation control should be developed to allow smoother movement of the wings and gradual actuation of each fin in a group of Pneufin shading. Other than that, more precise dynamic actuation test could be used to further access its actuation under wind load.

The sudden and imbalance movement of the wings shows the disadvantages of Pneufin compared to other SPAS. Some SPAS was designed for the intention of smooth, elegant, and/or biologically similar movement [18,28]. Emphasizing the smooth inflation of stretchable material, muscle like movement can be achieved by some SPAS [26]. But Pneufin actuated from folded to tightened position which does not have same characteristic. While this is a disadvantage of Pneufin, it begs the question of the importance of smooth movement for a building façade which rarely moves, and also expands the definition of soft pneumatic adaptive system itself.

4.2. Structure

The structural analysis also suggested the significancy of the middle layer membrane dimensions. It could be responsible to two unexpected result of the Prototype 2 Unfolded mode experiment: (1) the flipped correlation between the wing angle and wind to pneumatic pressure ratio, and (2) the stagnating pattern during the higher vacuum value. The Prototype 2 has smaller hoop stress angle of the Folded mode than the Prototype 1. Thus, it should have higher folding resistance during the Folded mode than the Prototype 1 too. This might be the cause of the first unexpected result of the Prototype 2 Unfolded mode experiment. The folding resistance were getting less as the wing angle increased, thus the wind to pneumatic pressure ratio increased and got closer to the simulation results.

The stagnating pattern during the higher vacuum value of the Prototype 2 Folded mode experiment could be due to the closer distance between the middle- and upper-layer membrane on the Prototype 2. Even though it was designed to still has around 3 cm space between the middle- and upper-layer membrane, something must have happened that the middle layer membrane stopped to pull the wing further at higher vacuum. The hypothesis of what happened was the flattening of the cap. As the vacuum increased, the cap was squeezed. Even if upper layer membrane was held in its place, the middle layer membrane might still be squeezed enough that could cause it to block the valve and not letting the air escape the tube (Fig. 19 right). The reason it happened only in the Prototype 2 might be due to its wider middle layer membrane.

The middle layer membrane (in the combination of lever and clamp stiffness) could also be the reason of curving pattern in 90° Unfolded mode structural experiment result of Prototype 1. Though at the first glance the Prototype 1 still has some room to wiggle before the middle layer membrane become straight, it only needs to expand by 2 mm to make it straight. Thus, it could be that pass certain pressure (around 4–5 kPA) the lever and clamp flex enough to straighten the middle layer membrane (Fig. 19 left).

This problem of middle layer membrane further emphasizes the non-linear behaviour of Pneufin. The similar problem could be seen in the forming of wrinkle and collapse of pneumatic structure [45]. Since Pneufin actuates from relaxed (collapse) state, it makes sense that it has the same problem.

The geometry of the clamp could also affect the structural performance. The significantly higher experiment result of the intermediate angles (45°–75°) Unfolded mode compared to its simulation could be due to the geometry of the clamps which were not

Fig. 18. Actuation of the aesthetic prototype.

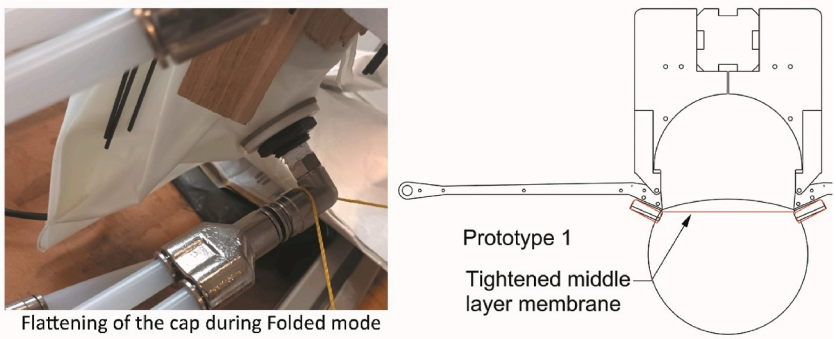

Fig. 19. Prototyping imperfections.

considered in the simulations. At these intermediate angles, the clamp pushes lower membrane. This could increase the lever moment arm, thus increasing the angular rigidity of the wing.

A simple analytical comparison was done on 45° Unfolded mode with and without considering the clamp geometry (Fig. 20). The pneumatic pressure used for the comparison was 10 kPa. The results of wind pressure were 317.71 PA for the no-clamp model and 502.53 PA for the clamped model. This clamped model has 58.17% higher wind pressure than the no-clamp model. It is a significant difference though it is still lower than the experiment result.

This study simplified the stiffness of the wing into its hinge angular moment. By finding the wind to pneumatic pressure ratio, the system inflates/vacuums up to the pressure which the wing would not rotate at its hinges. This method assumes that the wing does not flex during the loading. If the flexural of the wing and slight rotation on the hinges are considered during the loading, then the required pneumatic pressure could be more efficient. It might also introduce new problem of fluttering and fatigue. Thus, assessing the dynamic of the wing under wind load could be an important further study.

4.3. Building energy

The simulation shows that using Pneufin on west facing façade in tropical climate could decrease the total cooling and lighting electricity while keeps the daylight autonomy optimised. It also could be seen that adaptability of the Pneufin shading significantly affected the optimisation of the cooling, lighting, and daylight performance.

Even though cooling load is higher than the lighting electricity, adaptability of Pneufin shading effects the lighting and daylight autonomy more. It shows that there were more other variables (other than the Pneufin adaptability) that affects cooling load in these cases compared to the lighting and daylight autonomy.

Other than that, it could be because of the folded fin arrangement affect the daylight more than the heat gain. For example, solar radiation that hits corners of the zone would still add heating load to the zone but would not be useful for illumination. Two shading modes with same number of folded fins but different arrangements would likely to have same heat gain than having same illuminance effect to the building.

Together with façade aesthetic, and interior ambience, the adaptability and building energy reduction correlation would be an important note in the application of Pneufin since adding just one group could increase the complexity of inflation system.

There are several Pneufin façade parameters that could be explored to see its effect on building performance, such as the density of Pneufin, the wing shape, group arrangement, and the material properties. Evaluating this parameter could be important to decrease the dependency on Pneufin adaptability.

This study chose the control parameter of the Pneufin pragmatically since it is not the main aim of this study. Different parameter could be use as the setpoint such as daylighting. To implement the mode control from the simulation into real project would be to set the annual control schedule for Pneufin. But this would require initial forecasting and would be insensitive toward changes in the building and weather. Thus, how to implement the control into real project should also be evaluated.

4.4. Prototyping and fabrication

The prototyping in this study still focused for rapid prototyping and structural experiment. Nevertheless, the prototyping and the experiment has shown four critical components of Pneufin. Those are middle layer membrane, hinge, lever-clamp connection, wing, and the rigid upper chamber. Each of this component has different specification to be developed in addition to find the cost-effective method to fabricate.

The results showed that the most crucial layer of pneumatic tube is the middle one. It is important to find the optimal circumference, which both has less folding resistance and would not straighten under its intended max pressure. It should go hand in hand with the clamp and lever design and the dimension of the upper chamber.

Most critical rigid part of Pneufin would be around its hinges. As shown in the aesthetic prototype, most likely the rotation would be stopped around its hinge, especially during the Unfolded mode (Fig. 21). This also means that the load on hinge in real-world application would be higher than the hinge load in this experiment. Thus, the hinge would need to be the strongest part of Pneufin. Meanwhile the hinge should be able to withstand multiple actuations without wearing.

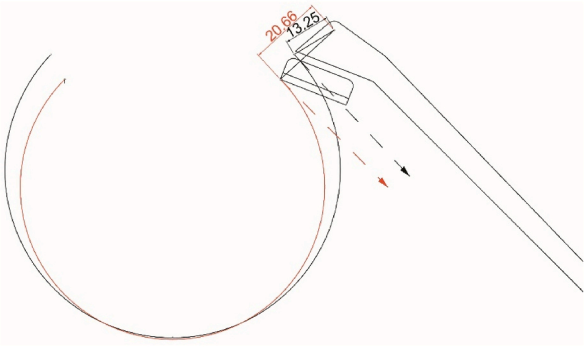

Fig. 20. Rigid body schematic with and without clamps.

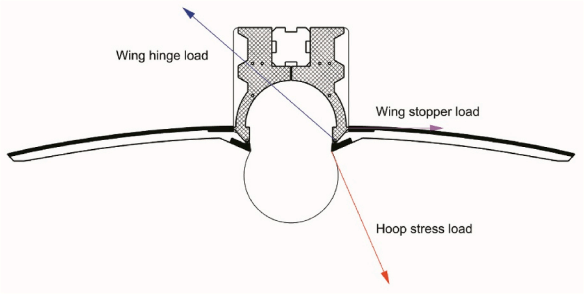

Fig. 21. Hinge load schematic.

Similar with the hinge, the lever and clamp would also need to be rigid. Increasing the number of hinges could decrease both load on hinge and lever-clamp. But how it would affect the friction and weight also needs to be seen.

The upper layer needs to be rigid and airtight. In addition, it is also needs to be slack around the hinges to make sure it would not apply load to the lever. The upper layer also supports the whole weight of Pneufin. All these requirements must be optimised with its slimness since it is at the front of Pneufin. The same principle as the prototypes could be used which is by clamping a membrane with two pieces of rigid component. The outer rigid component could be replaced by slightly bigger half tube instead of 3D printed part used in this research.

5. Conclusion

This study shows that the principle of Pneufin does enable soft pneumatic adaptive structure with low actuation pressure. The experiment shows that Pneufin could be actuated to both modes with low pressure ($<$1 kPa). The actuation pressure was affected by the friction of the hinge, and the folding resistance of the membrane.

The wing angular rigidity of Pneufin correlates with its pneumatic pressure. This means that the pneumatic pressure only needs to be increased if there is an increase in wind load. Due to the smaller chamber radius, Folded mode would have lower wind to pneumatic pressure ratio than the Unfolded mode.

But the experiment showed that middle layer membrane significantly affected this performance at both modes. In both modes, the linear correlation of pneumatic to wind pressure have the tendency to stagnate at higher pressure or vacuum. In Folded mode, the bigger the middle layer membrane the higher the chance of the stagnation. Reversely, the shorter the middle layer membrane the easier for the it to straighten during the Unfolded mode and hinder the actuation at higher pressure. Thus, finding the optimised middle layer membrane dimension according to its use would be very important.

This study showed that the use of Pneufin could decrease the building energy and increasing the Pneufin adaptability could increase this building energy reduction. The adaptability also affects the daylight autonomy optimisation without sacrificing the building energy reduction.

Pneufin developed in this research is still in a form of vertical external shading on building facade. Different use of Pneufin principle could be further studied, such as horizontal external shading on building façade or under skylight. Other than that, the same actuation principle used in switchable multilayer cushion foil structure could be implemented on a different form other than Pneufin.

Alongside its fabrication, the full implementation of Pneufin is also an important further study for Pneufin, especially in regards of its economic efficiency. The fabrication, construction, and inflation system of Pneufin would affect its implementation cost. Even though Pneufin does not need high pressure to actuate, its total system volume and its leakage would still affect the operation energy. A complete set of Pneufin façade operated on long period of time would be needed to evaluate this aspect.

CRediT authorship contribution statement

Rakhmat Fitranto Aditra: Conceptualization, Methodology, Software, Formal analysis, Investigation, Writing – original draft, Writing – review & editing. **Paolo Beccarelli:** Supervision, Writing – review & editing. **Robin Wilson:** Supervision, Writing – review & editing.

Declaration of competing interest

The authors declare that they have no known competing financial interests or personal relationships that could have appeared to influence the work reported in this paper.

Data availability

Data will be made available on request.

Acknowledgment

This work was funded by Indonesia Endowment Fund for Education (LPDP) under Indonesian Ministry of Finance as part of author's PhD thesis research.

Appendix A. Supplementary data

Supplementary data to this article can be found online at https://doi.org/10.1016/j.jobe.2023.107521.

References

[1] A. Zarzycki, M. Decker, Climate-adaptive buildings: systems and materials, Int. J. Architect. Comput. 17 (2019) 166–184, https://doi.org/10.1177/1478077119852707.
[2] Branko Kolarevic, V. Parlac, ADAPTIVE, responsive building SKINS, in: Build. Dyn. Explor. Archit. Chang., Routledge, London, 2015, https://doi.org/10.4324/9781315763279.
[3] S. Li, H. Fang, K.W. Wang, Recoverable and programmable collapse from folding pressurized origami cellular solids, Phys. Rev. Lett. 117 (2016) 1–5, https://doi.org/10.1103/PhysRevLett.117.114301.
[4] C.H. Annette Bögle, Mike Schlaich, C. Hartz, Pneumatic structures in motion, in: Evol. Trends Des. Anal. Constr. Shell, Spat. Struct., 2010, pp. 2019–2030.
[5] L. R, Climate Adaptive Building Shells, what Can We Simulate? Technische Universiteit Eindhoven, 2010.
[6] J. Lv, L. Tang, W. Li, L. Liu, H. Zhang, Topology optimization of adaptive fluid-actuated cellular structures with arbitrary polygonal motor cells, Smart Mater. Struct. 25 (2016), https://doi.org/10.1088/0964-1726/25/5/055021.
[7] G. Schieber, L. Born, P. Bergmann, A. Körner, A. Mader, S. Saffarian, O. Betz, M. Milwich, G.T. Gresser, J. Knippers, Hindwings of insects as concept generator for hingeless foldable shading systems, Bioinspiration Biomimetics 13 (2018), https://doi.org/10.1088/1748-3190/aa979c.
[8] Z. Nagy, B. Svetozarevic, P. Jayathissa, M. Begle, J. Hofer, G. Lydon, A. Willmann, A. Schlueter, The adaptive solar facade: from concept to prototypes, Front. Archit. Res. 5 (2016) 143–156, https://doi.org/10.1016/j.foar.2016.03.002.
[9] Corolla (Milan, 2019) (n.d.), http://albaghuba.com/?p=53. (Accessed 14 May 2020).
[10] R. Velasco, A.P. Brakke, D. Chavarro, Dynamic façades and computation: towardsan inclusive categorization of high PerformanceKinetic façade systems, in: CAAD Futur. Proc. Comput. Archit. Des. Futur. Next City - New Technol. Futur. Built Environ, 2015, pp. 172–191, https://doi.org/10.1007/978-3-662-47386-3, 2015.
[11] G.E. Fenci, N.G.R. Currie, Deployable structures classification: a review, Int. J. Space Struct. 32 (2017) 112–130, https://doi.org/10.1177/0266351117711290.
[12] R.C.G.M. Loonen, M. Trčka, D. Cóstola, J.L.M. Hensen, Climate adaptive building shells: state-of-the-art and future challenges, Renew. Sustain. Energy Rev. 25 (2013) 483–493, https://doi.org/10.1016/j.rser.2013.04.016.
[13] A.E. Del Grosso, P. Basso, Adaptive building skin structures, Smart Mater. Struct. 19 (2010), https://doi.org/10.1088/0964-1726/19/12/124011.
[14] M. López, R. Rubio, S. Martín, Croxford Ben, How plants inspire façades. From plants to architecture: biomimetic principles for the development of adaptive architectural envelopes, Renew. Sustain. Energy Rev. 67 (2017) 692–703, https://doi.org/10.1016/j.rser.2016.09.018.
[15] A. Lanza Volpe, Building optimization: the adaptive façade, Adv. Mater. Res. 1149 (2018) 64–75. https://doi.org/10.4028/www.scientific.net/amr.1149.64.
[16] A. Tabadkani, A. Roetzel, H.X. Li, A. Tsangrassoulis, Design approaches and typologies of adaptive facades: a review, Autom. ConStruct. 121 (2021), 103450, https://doi.org/10.1016/j.autcon.2020.103450.
[17] S.M. Hosseini, M. Mohammadi, A. Rosemann, T. Schröder, J. Lichtenberg, A morphological approach for kinetic façade design process to improve visual and thermal comfort: review, Build. Environ. 153 (2019) 186–204, https://doi.org/10.1016/j.buildenv.2019.02.040.
[18] D. Andrić, J. Galić, K. Šerman, Actuation characteristics of basic body plans for soft modular pneubotics in architecture, Buildings 11 (2021), https://doi.org/10.3390/buildings11030106.
[19] A. Gómez-González, J. Neila, J. Monjo, Pneumatic skins in architecture. Sustainable trends in low positive pressure inflatable systems, Procedia Eng. 21 (2011) 125–132, https://doi.org/10.1016/j.proeng.2011.11.1995.
[20] R. Aditra, P. Beccarelli, C. Jimenez-Bescos, Switching Transformation for Soft Pneumatic Adaptive Shading, 2021, pp. 1–10, https://doi.org/10.23967/membranes.2021.020.
[21] B. Gramüller, J. Boblenz, C. Hühne, Pacs - realization of an adaptive concept using pressure actuated cellular structures, Smart Mater. Struct. 23 (2014), https://doi.org/10.1088/0964-1726/23/11/115006.
[22] L. Born, A. Körner, G. Schieber, A.S. Westermeier, S. Poppinga, R. Sachse, P. Bergmann, O. Betz, M. Bischoff, T. Speck, J. Knippers, M. Milwich, G.T. Gresser, Fiber-reinforced plastics with locally adapted stiffness for bio-inspired hingeless, deployable architectural systems, 742 KEM, Key Eng. Mater. (2017) 689–696, https://doi.org/10.4028/10.4028/www.scientific.net/KEM.742.689.
[23] D. Park, M. Bechthold, Designing biologically-inspired smart building systems: processes and guidelines, Int. J. Architect. Comput. 11 (2013) 437–463. https://doi.org/10.1260/1478-0771.11.4.437.
[24] J.F. Flor, D. Liu, Y. Sun, P. Beccarelli, J. Chilton, Y. Wu, Optical aspects and energy performance of switchable ethylene-tetrafluoroethylene (ETFE) foil cushions, Appl. Energy 229 (2018) 335–351, https://doi.org/10.1016/j.apenergy.2018.07.046.

[25] M. Decker, Soft robotics and emergent materials in architecture, in: ECAADe 2015 Real Time - Proc. 33rd Int. Conf. Educ. Res. Comput. Aided Archit. Des. Eur. 2, 2015, pp. 409–416. http://papers.cumincad.org/cgi-bin/works/Show?ecaade2015_178.
[26] M. Kim, B. Kim, J. Koh, H. Yi, Flexural biomimetic responsive building façade using a hybrid soft robot actuator and fabric membrane, Autom. ConStruct. 145 (2023), 104660, https://doi.org/10.1016/j.autcon.2022.104660.
[27] L. Tomholt, O. Geletina, J. Alvarenga, A.V. Shneidman, J.C. Weaver, M.C. Fernandes, S.A. Mota, M. Bechthold, J. Aizenberg, Tunable infrared transmission for energy-efficient pneumatic building façades, Energy Build. 226 (2020), 110377, https://doi.org/10.1016/j.enbuild.2020.110377.
[28] C. Eisenbarth, W. Haase, Y. Klett, L. Blandini, W. Sobek, PAOSS : pneumatically actuated origami sun shading, J. Facade Des. Eng. 9 (2021) 147–162, https://doi.org/10.7480/jfde.2021.1.5535.
[29] R. Vos, R. Barrett, Mechanics of pressure-adaptive honeycomb and its application to wing morphing, Smart Mater. Struct. 20 (2011), https://doi.org/10.1088/0964-1726/20/9/094010.
[30] Grasshopper® (n.d.), https://www.grasshopper3d.com/.
[31] RFEM Dlubal (n.d.), https://www.dlubal.com/en-US/products/rfem-fea-software/what-is-rfem. (Accessed 3 August 2021).
[32] Honeybee (n.d.), https://www.ladybug.tools/honeybee.html. (Accessed 3 August 2021).
[33] Badan Standarditasi Nasional (BSN), SNI 6389:2011, Tentang Konservasi Energi Selubung Bangunan Pada Bangunan Gedung, 2011, pp. 1–60.
[34] W. Sujatmiko, H.K. Dipojono, F.X. Nugroho Soelami, Soegijanto, *in situ* measurement of thermal resistance of building envelope at the residential occupancy in Indonesia, Appl. Mech. Mater. 771 (2015) 191–194. https://doi.org/10.4028/www.scientific.net/amm.771.191.
[35] Jakarta Provincial Government, Jakarta Green Building User Guide: Building Envelope, 2016, p. 1. http://greenbuilding.jakarta.go.id/.
[36] CLASP Environmental Design Solutions, Indonesia Refrigerator Market Study and Policy Analysis, 2020, pp. 1–108.
[37] IEA, Lighting, Paris, https://www.iea.org/reports/lighting, 2021.
[38] B.L. Ahn, C.Y. Jang, S.B. Leigh, S. Yoo, H. Jeong, Effect of LED lighting on the cooling and heating loads in office buildings, Appl. Energy 113 (2014) 1484–1489, https://doi.org/10.1016/j.apenergy.2013.08.050.
[39] K. Gordon, Thermal Management of White LEDs, US. Dep. Energy, 2007, pp. 10–11. http://apps1.eere.energy.gov/buildings/publications/pdfs/ssl/thermal_led_feb07_2.pdf.
[40] B.S. Nasional, SNI 03-6197-2000 Konservasi Energi Pada Sistem Pencahayaan, Sni 03-6197-2000, 2000, p. 17.
[41] BSN, SNI - 03 - 6572 - 2001,Tata Cara Perancangan Sistem Ventilasi Dan Pengkondisian Udara Pada Bangunan Gedung, 2003, pp. 1–55. http://staffnew.uny.ac.id/upload/132100514/pendidikan/perencanaan-pendingin.pdf.
[42] IEA, The future of cooling in southeast Asia, futur. Cool. Southeast Asia. https://www.iea.org/reports/the-future-of-cooling-in-southeast-asia, 2019.
[43] ASHRAE, ASHRAE Handbook of Fundamentals, 2017.
[44] T. Becker, Breathing skins. https://www.tebe.berlin/breathing-skins/, 2015. (Accessed 12 June 2023).
[45] J.C. Thomas, A. Bloch, Non linear behaviour of an inflatable beam and limit states, Procedia Eng. 155 (2016) 398–406, https://doi.org/10.1016/j.proeng.2016.08.043.